Characterization of Vertically Aligned Carbon Nanofibers Without Electrochemical Treatment Using Atomic Force Microscopy

Zhuxin Dong, *Student Member, IEEE*, and Uchechukwu C. Wejinya, *Member, IEEE*

***Abstract*—One of the major limitations in the development of ultrasensitive electrochemical biosensors based on 1-D nanostructure is the difficulty involved with reliably fabricating nanoelectrode arrays. In the previous work (Arumugam *et al.*, 2009), a simple, robust, and scalable wafer-scale fabrication method to produce multiplexed biosensors was introduced. Each sensor chip consists of nine individually addressable arrays that uses electron-beam patterned vertically aligned carbon nanofibers (VACNFs) as the sensing element. To ensure nanoelectrode behavior with higher sensitivity, VACNFs were precisely grown on 100 nm Ni dots with 1 μm spacing on each micropad. However, in order to examine the quality and measure the height and diameter of the VACNFs, some surface detection and measurement tool at the nanoscale level is needed. In this paper, we introduce an approach to measure these nanoscale features through atomic force microscope. With this method, both the 2-D and 3-D images of sample surface are generated and the sizes of carbon nanofibers and cavities are obtained. Furthermore, statistical analysis is carried out to enable the improvement of VACNFs' growth and fabrication.**

***Index Terms*—Atomic force microscopy (AFM), biosensors, chemical sensors, nanoelectrodes, statistical nanotechnology.**

I. Introduction

With RECENT increase in pathogen outbreaks in water, food, and other media, new methods and technologies for detection and quantification are needed. These devices and systems will need to be fast, reliable, ultrasensitive, portable, and automated. For several decades, detection heavily relied upon an indicator organism approach to assess the microbiological quality of drinking water. However, an increased understanding of the diversity of waterborne pathogens has concluded that the use of bacterial indicators may not be as universally protective as was once thought [2]. Newer methods involving immunofluorescence techniques and nucleic acid analysis provide valuable opportunities for rapid and more specific analytical methods. Particularly, electrochemical (EC) biosensors are attractive for detecting a wide range of species including proteins, nucleic acids, small molecules and viruses because of their relative simplicity, portability, low cost, and low power requirement. EC biosensors consist of two primary components: a recognition layer containing a biomolecule and an EC signal transducer. They make use of EC reactions or the surface property changes upon target binding. Advances in microfabrication technology have provided electrode configurations such as microelectrode arrays [3] and interdigitated arrays (IDA) [4], but their performance can be further enhanced by miniaturizing to nanoscale. Recent progress in nanofabrication technologies like electron-beam lithography and nanoimprinting enable fabrication of 1-D nanostructure electrodes like carbon nanofibers [5]–[7], carbon nanotube bundles [8], [9], nanoscale IDA [10], silicon nanowires [11], and diamond nanowires [12], which are capable of high spatial and temporal resolutions, possibly yielding sufficient sensitivity to single molecule detection. Among various types of 1-D nanoscale electrodes, vertically aligned carbon nanofibers (VACNFs) have received tremendous attention because of their attractive properties such as high electrical and thermal conductivities, superior mechanical strength, a wide EC potential window, flexible surface chemistry, and biocompatibility [13], [14]. Compared to other carbon materials such as glassy carbon, carbon black, carbon microfibers, and pyrolytic graphite, the open-ended VACNF arrays present well-defined edgeplane structure suitable for selective covalent functionalization of primary amine-terminated oligonucleotide probes. Thus, the microchip, a 3×3 array biosensor using nanopatterned VACNF array for detection of chemical particles, such as *E. coli* O157:H7, has been achieved [1]. However, to examine how well the growth of the VACNFs is, an advanced measurement and characterization tool such as the atomic force microscope (AFM) is employed.

AFM is a very high-resolution type of scanning probe microscope that has resolution of fractions of a nanometer. The AFM was created specifically to generate a 3-D view of a scanned object, unlike the SEM that can only produce 2-D views. With the ability to scan almost any type of surface, the AFM is used in many types of research. Surfaces include polymers, ceramics, composites, glass, and biological samples. The AFM also has a variety of operation modes including contact mode, lateral-force microscopy, noncontact mode, tapping mode, and phase imaging. This feature induces the stunning capabilities of this microscope by only applying a simple set of modifications. The microscope uses a microscale cantilever with a probe at the end that is used to scan a surface. A beam-deflection system consisting of a laser and photodetector is built into the microscope to measure the position of the beam and, ultimately, the position of the cantilever tip. In order to calculate the force, Hooke's Law

Manuscript received March 22, 2010; accepted June 1, 2010. Date of publication July 23, 2010; date of current version May 11, 2011. The review of this paper was arranged by Associate Editor L. Dong.

The authors are with the Department of Mechanical Engineering, University of Arkansas, Fayetteville, AR 72701 USA (e-mail: dzhuxin@uark.edu; uwejinya@uark.edu).

Digital Object Identifier 10.1109/TNANO.2010.2060346

$F = -kz$, where F is the force, k is the spring constant of the cantilever, and z is the displacement of the cantilever, is used. The laser beam is placed on the cantilever tip and the beam deflection measures the displacement the sample exerts on the cantilever. The spring constant is known based on what type of scanning probe is used. With its 3-D capabilities and ability to operate in air and liquid rather than a vacuum-sealed environment, the AFM aids many studies in biological macromolecules, tribiology, and optical and imaging sciences. The microscope has the capabilities of scanning living organisms through the study of measurements of protein–ligand interactions on living cells and many other research applications. The AFM has been used as the primary microscope in the direct measurement of interatomic force gradients, detection, and localization of single molecular recognition events, single molecule experiments at the solid–liquid interface and fractured polymer/silica fiber surface research. Owing to the aforementioned advantages, the AFM is capable of completing the dimensional analysis of the nanofibers and cavities.

After the acquisition of the size data, some specified statistical analysis is applied. Confidence interval (CI) and p value are employed to provide us with a reliable size range and a judgment of the truth of future measurement after taking the current information as a standard. Finally, a conclusion is able to be reached to summarize and examine the size of these VACNFs without any EC treatment.

II. Fabrication of Nanoelectrode

The intensively sensitive fabrication process of VACNF nanoelectrode arrays (NEAs) includes six major steps done on a four-inch silicon (100) wafer that was previously coated with 500 nm of silicon dioxide. The steps of the fabrication process as well as the corresponding SEM images are shown in Figs. 1 and 2, respectively. The steps include 1) metal deposition for micropads, contact pads, and electrical interconnects; 2) nanopatterning of Ni catalyst dots; 3) directional growth of CNFs; 4) silicon-dioxide deposition for electrical isolation and mechanical support; 5) chemical mechanical polishing (CMP) to expose CNF tips; and 6) a wet etch with 7:1 HF to expose contact pads.

A. Deposition of Metal

Using optical-lithography patterning, 30 chips are able to be patterned onto the four-inch wafer. Each chip contains nine contact pads that are attached by electrical interconnects to a single 3×3 set of arrays. Each of the nine arrays and the contact pads measures 200×200 μm^2 and 2×2 cm^2, respectively. Electrically, the underlying oxide isolates the pads. Using a 1-μm-thick Shipley 3612 resist and microlithography, the pads and interconnects are patterned. An inspection under a microscope is made and then the patterns were metalized using a lift-off technique. The process of electron-beam evaporation is then used to deposit a 200 nm thick Cr film and then the wafer is immersed in acetone for 1 h. Once removed from the acetone, the wafer is sprayed with methanol and isopropyl alcohol (IPA) and blown dry with N_2.

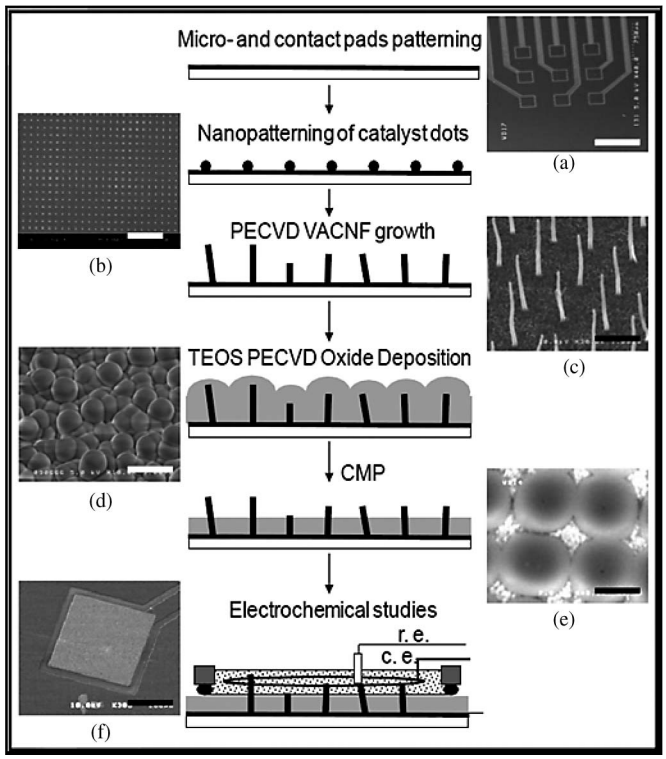

Fig. 1. Procedure of fabricating biosensors based on nanopatterned VACNFs: (a) deposition of metal; (b) nanopatterning; (c) growth of CNFs; (d) deposition of silicon dioxide; (e) chemical mechanical polishing; and (f) electrochemical characterization.

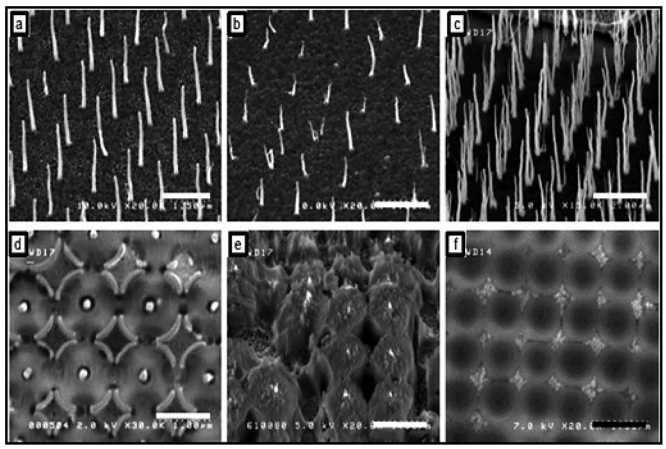

Fig. 2. Top row shows the importance of PECVD chamber conditioning on CNF growth: (a) final run in "warm chamber"; (b) initial run in "cold chamber"; (c) effect of high thermal ramps ($\sim$200 °C/min) resulting in multiple fibers from single nanopot. Bottom row illustrates SEM images of patterned arrays after re-exposing VACNF tips by reactive ion etching (d), (e) and CMP (f). The dots are 100 nm in diameter and 1 μm in spacing.

B. Nanopatterning

Catalyst dots are then added to the wafer via a process called electron-beam lithography patterning. There are approximately 39000 catalyst dots that measure 100 nm in diameter on each micropad. The process begins with spinning a 400-nm-thick layer of polymethyl methacrylate onto the wafer and then baking it at 180 °C for 90 s and then exposed at 100 keV, 2 nA,

1950 μC/cm^2. After immersing the exposures into a solution of half methyl isobutyl ketone and half IPA for 2 min, and then IPA for 30 s, the exposures are developed. The wafer is then blown dry with N_2 and examined under a microscope and again the pattern is metalized using a lift-off technique. The process of electron-beam evaporation is then used to deposit a 10-nm-thick film of Cr trailing with a 30-nm-thick layer of Ni catalyst. The wafer was then submerged in acetone for 1 h. After the time elapsed, the wafer is removed and sprayed with IPA and N_2 to blow dry.

C. Growth of VACNFs

The next step is growing the VACNFs on the nickel dots that are created in step *B*. The growth is dc-biased plasma enhanced chemical vapor deposition (PECVD) growth. At a processing pressure of 6.3 mbar, plasma power of 180 W and 700 °C, 125 sccm C_2H_2 feedstock, and 444 sccm NH_3 diluent are initiated. Then, a 5 min thermal annealing at 600 °C is carried out following with 250 sccm NH_3. To attain the growth temperatures and thermal anneal needed, a 60 °C/min incline is used. Each individual CNF is vertically arranged to freestand on the surface with Ni catalyst on each tip. To check and affirm the process is done correctly, a 15 min deposition is conducted. Average results include a height of 1.5 μm, 100 nm base diameter, and 70 nm tip diameter. The uniformity of the growth is then checked by SEM.

D. Deposition of Silicon Dioxide

PECVD of silicon dioxide is managed next. To passivate the sidewalls of each individual fiber, a 3 μm SiO_2 layer is deposited onto the wafers using a pressure of 3 Torr, temperature of 400 °C and RF power of 1000 W. The process includes a parallel plate, dual RF, PECVD using a mixture of 6000 sccm of O_2 and 2–3 mL/min of tetraethlyorthosilicate (TEOS). A highly conformal coating of SiO_2 is created on the newly created fibers and interconnects.

E. Chemical Mechanical Polishing

By CMP, existing of stock removal and final polish, the overrun oxide, and a portion of the VACNFs are removed. This process involves removing the existing material with 0.5 μm alumina (pH 4) at 10 mL/min, 60-r/min platen, 15-r/min carrier, and 15 psig down force at 150 nm/min, re-exposure of VACNF tips and surface planarization. A 0.1 μm alumina (pH 4) at 10 mL/min, 60-r/min platen, 15-r/min carrier, and 25 psig down force is operated for final polish at 20 nm/min. The wafer is cleaned by immersing it into a solution composed of water, hydrogen peroxide, and ammonium hydroxide at a ratio of 80:2:1, respectively, and then spin-dried. The aim to re-expose the VACNF tips is carried out as well as the planarization of the surface.

F. Wet Etch

To expose the contact pads, a careful etching using silicon dioxide is achieved. Optical lithography, using 2.5-μm-thick Shipley 3012 resist, is again used to remove SiO_2 from the contact pads for electrical connections to the potentiostat. The Shipley resist is baked at 125 °C for 120 s and immediately immersed in Shipley EC11 to be exposed and developed. The wafer is then rinsed using deionized (DI) water and inspected via a microscope. Then, to set the resist, the wafer is baked at 125 °C for 180 s. Then, using a 7:1 diluted HF solution, the oxide is carefully etched off of the contact pads at approximately 15 Å/s. For 15 min, the resist is then stripped off of the wafer using EKC 830 resist stripper. The wafer is then rinsed with DI water, blown dry with N_2 and diced into 30 individual chips sized approximately 14 mm^2.

III. Experimental Setup

In order to accurately determine the height and diameter of the VACNFs grown on 100 nm Ni dots, an AFM is employed. The AFM used in the experiment is the Agilent 5500-ILM highly sensitive microscope as shown in Fig. 3, which illustrates the experimental setup: the scan target is a single chip which contains 1×9 contact pads and a 3×3 set of NEAs. Each of these electrode arrays has a 200×200 μm^2 area. The scanning will be done under Acoustic ac imaging mode, which is intermittent contact or noncontact as shown in Fig. 4, and the AFM probe has a resonant frequency of 190 kHz and a spring constant of 48 N/m. As introduced in the AFM manual, during intermittent contact, the tip is brought close to the sample so that it lightly contacts the surface at the bottom of its travel, causing the oscillation amplitude to drop. Hence, we may completely ignore the influence of the cantilever tip during the size measurement, as it cannot change anything of the target shape without contacting.

IV. Experimental Result

A. Scanning and Measurement

Before measuring the size of the VACNFs and the cavities on the NEAs, they should be located and observed. Thus, we scan the arrays from a 9×9 μm^2 area in the middle of the chip. After locating the fibers and cavities, we can zoom into a 2×2 μm^2 area, which encloses the identified fiber tips and cavities to obtain clear scan image and guarantee a better and more accurate measurement. When a fiber or cavity appears clear in a scan topography image, a straight line can be drawn in any direction in the 2-D topography image to cross the target. At the same time, we can obtain the vertical information all the way along the line to complete a measurement. This procedure is repeated until sufficient data is obtained for a particular array before starting on a new array of nanofibers. Take Array 1 for instance: Fig. 5 illustrates a topography scan in a 9×9 μm^2 area of the array. As we can see, under such a scale only cavities are obvious. However, that is enough as we can zoom in to find fiber tips surrounding the cavities. Fig. 6 shows a zoomed-in topography in 2×2 μm^2 area. Besides a single cavity, there are four fiber tips surrounding that cavity. For a better view, a 3-D image of this topography scan is generated as shown in Fig. 7. These cavities are caused by the chemical tetraethlyorthosilicate (TEOS), which is applied during the step of PECVD oxide

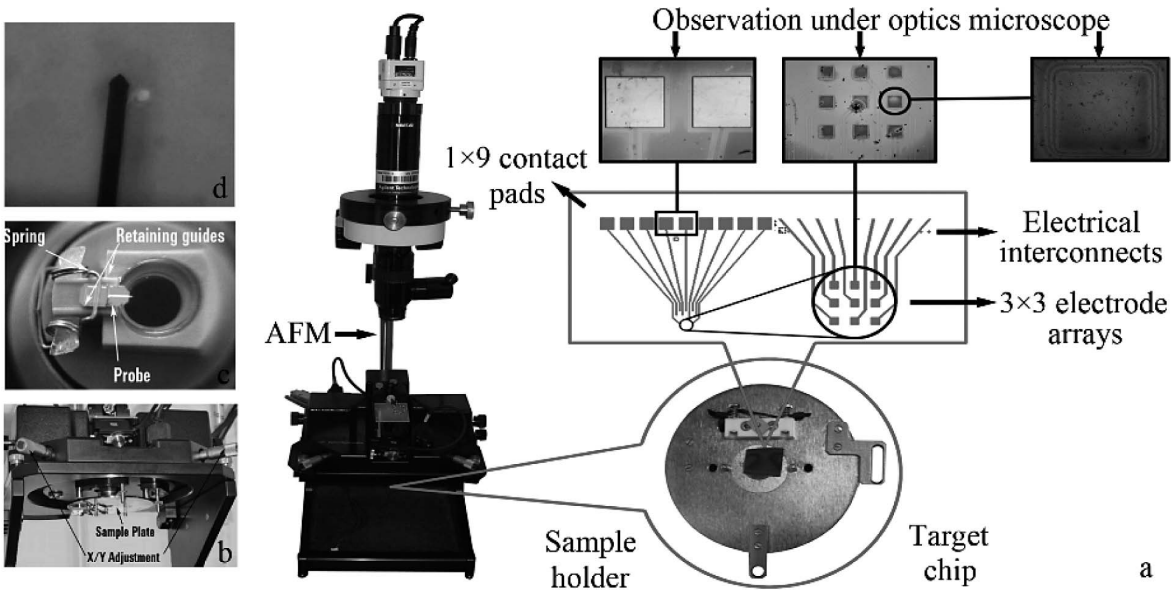

Fig. 3. Experimental setup for scanning and measurement based on AFM: (a) main system structure; (b) sample holder on microscope stand; (c) probe properly situated on AFM nose assembly; and (d) using video system to align laser.

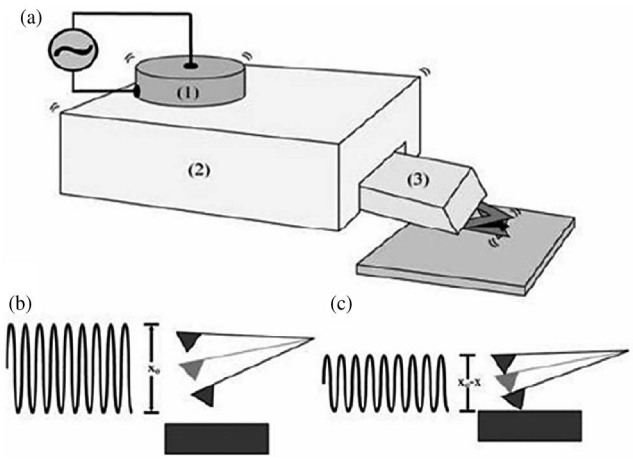

Fig. 4. AFM probe motion under Acoustic AC Mode: (a) (1) AC applied to the nosecone; (2) the base body of the cantilever beam; (3) the cantilever bean with its tip; (b) and (c) the cantilever driven to oscillate in sinusoidal motion.

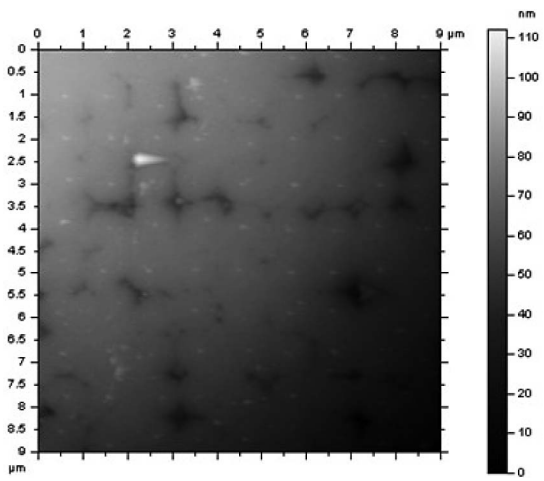

Fig. 5. $9 \times 9\ \mu m^2$ topography scan of Array 1 Chip 1: cavities are located.

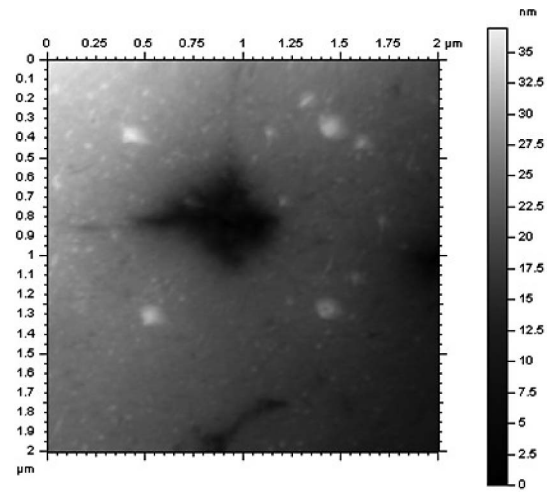

Fig. 6. Zoomed-in topography scan image of Array 1 in $2 \times 2\ \mu m^2$ area: both cavity and fiber tip are found. So it is ready to measure.

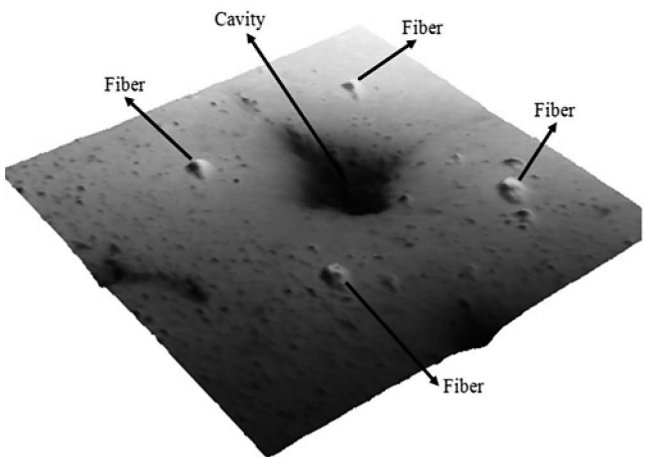

Fig. 7. 3-D image generated for a better view based on Fig. 6.

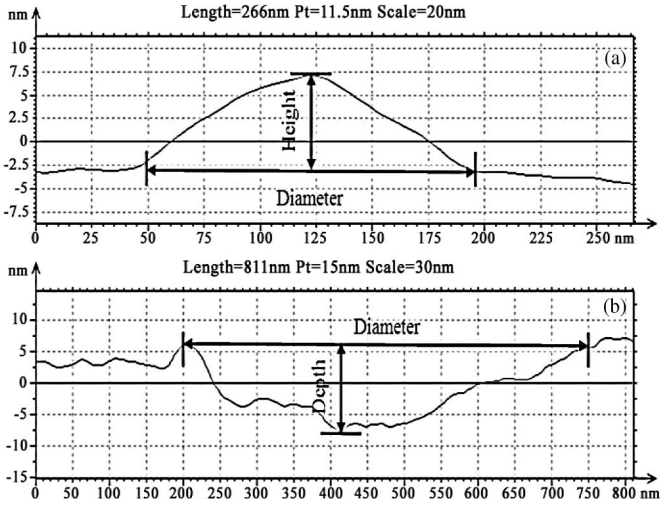

Fig. 8. Cross section information for measurement based on the line drawn crossing (a) a fiber and (b) a cavity in Fig. 7.

deposition. Thus, the measurement can be done by drawing lines crossing the cavities and the fiber tips. Fig. 8 illustrates how to obtain the height and diameter of a fiber tip and the depth and diameter of a cavity from a cross-sectional image.

Table I gives the measurement results in detail by obtaining ten measured values of fiber size consisting of diameter and height for each array and the mean values are shown in Fig. 9. Besides the fibers, five measurements of the cavities for each array in this chip are completed and their mean values are shown in Fig. 10. In addition, we repeated the same measurement procedure for fibers on a second chip, which is fabricated the same way, and the result is illustrated in Fig. 11. After the mean values of the diameter and height of the fibers in each array on both Chip 1 and Chip 2 are obtained, in order to describe the size more accurately, statistical analysis is employed.

TABLE I
RESULT OF MEASUREMENT FOR FIBERS ON CHIP 1

Chip 1	Array 1		Array 2		Array 3	
Meas. #	Diam.	Height	Diam.	Height	Diam.	Height
1	121.43	11	159.64	8.2	164.52	6.8
2	133.18	6.3	139.68	8.1	156.68	5.1
3	129.26	10.7	123.72	6.5	141.01	8.1
4	121.43	5.8	123.72	9.6	164.51	5.4
5	137.1	9.6	137.09	8	152.78	9.1
6	144.93	6	160.6	6.2	133.56	8.4
7	125.34	6.7	148.85	7.7	144.93	10.2
8	148.85	7	156.68	7.5	125.34	10.3
9	137.09	10.2	166.72	9.9	144.99	6.3
10	117.51	6.7	146.34	6.6	117.71	6.4
	Array 4		**Array 5**		**Array 6**	
	Diam.	**Height**	**Diam.**	**Height**	**Diam.**	**Height**
1	164.53	8.8	144.93	10.9	144.94	7.4
2	168.45	7.6	164.53	8.9	156.75	7.3
3	129.26	6.7	168.44	8.8	148.85	8.4
4	156.68	5.8	160.64	8.4	129.28	8
5	152.53	5.7	161.43	6.1	143.65	6.1
6	155.65	8	153.72	7.5	139.65	7.4
7	163.63	8.2	157.59	7.2	167.59	6.6
8	151.66	6.8	146.06	10	119.72	8.1
9	141.02	9.7	164.54	6.6	152.77	6.8
10	144.93	8.2	148.93	9.3	164.56	6.6
	Array 7		**Array 8**		**Array 9**	
	Diam.	**Height**	**Diam.**	**Height**	**Diam.**	**Height**
1	135.69	8	139.7	7.6	141.02	7.4
2	143.7	9.1	143.74	7.8	141.02	5.6
3	127.71	6.4	147.67	9.7	129.28	7.1
4	119.75	7.3	151.67	10.9	125.34	7.4
5	121.43	8.2	141.01	9.3	148.85	6
6	117.54	7.8	144.93	7.1	137.12	6.4
7	129.26	6.2	145.04	7.7	133.18	6.6
8	134.29	7.5	133.18	10.2	141.03	6.4
9	117.51	6.4	129.37	7.3	143.69	7.7
10	137.12	5.8	129.35	9.2	135.69	7.2
Overall Mean			**Diameter: 142.87**		**Height: 7.7**	

All measured values are in the unit of nanometer.

B. Statistical Analysis

1) Confidence Interval: In statistics, a CI is an interval estimate of a population parameter [15]. Instead of estimating the parameter by a single value, an interval likely to include the parameter is given. Thus, CIs are used to indicate the reliability of an estimate. How likely the interval is to contain the parameter is determined by the confidence level or confidence coefficient.

Therefore, we apply this statistical method to our experiment to obtain the interval to describe the size of fibers. Take the fibers in Chip 1, for instance, from Table I and Fig. 9, the mean values for each array are obtained and we put the value as the first element in a 1×9 matrix as follows: {131.61 146.3 144.6 152.83 157.08 146.78 128.4 140.57 137.62}, and then we substitute these samples into the calculation of a 95% CI. The mean of the matrix is 142.87 nm and the standard deviation is 8.82 nm. Thus, the CI is determined as [137.11 nm 148.63 nm]. For the height, the matrix is as follows: {8 7.83 7.61 7.55 8.37 7.27 7.27 8.68 6.78}, the mean is equal to 7.7 nm and the standard deviation is 0.554 nm. Thus, the CI can be determined as [7.338 nm 8.062 nm]. Furthermore, based on the data in Fig. 10, the standard deviations are 66.65 and 2.07 nm for cavity diameter and depth, respectively. Thus, the 95% CIs can be calculated to describe the diameter and depth as [453.03 nm 540.12 nm] and [8.46 nm 11.16 nm], respectively. Finally, from Fig. 11, another two CIs with same confidence level are computed, [143.13 nm 153.17 nm] and [7.18 nm 8.62 nm] for diameter and height, respectively. Their standard deviations are 7.68 and 1.11 nm, respectively. Hence, the accurate size of the fibers and cavities can be determined with the intervals as stated. The CI result details are given in Table II and (1) shows how to calculate the interval

$$\mathrm{CI} = \left[\bar{X} - Z \times \frac{\sigma}{\sqrt{N}}, \bar{X} + Z \times \frac{\sigma}{\sqrt{N}}\right] \tag{1}$$

where $\bar{X}$ is the mean values of the samples, Z is the critical value equal to 1.96 in a 95% CI, σ is the standard deviation, and N is the number of the samples.

2) P Value: Besides CI, another statistical method is employed to help, p value. In statistical hypothesis testing, the p value is the probability of obtaining a test statistic at least as extreme as the one that was actually observed, assuming that

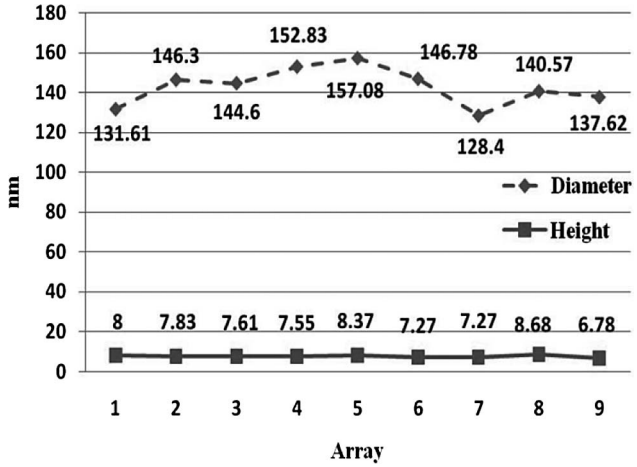

Fig. 9. Measurement result of fiber size in Chip 1 presented by mean values.

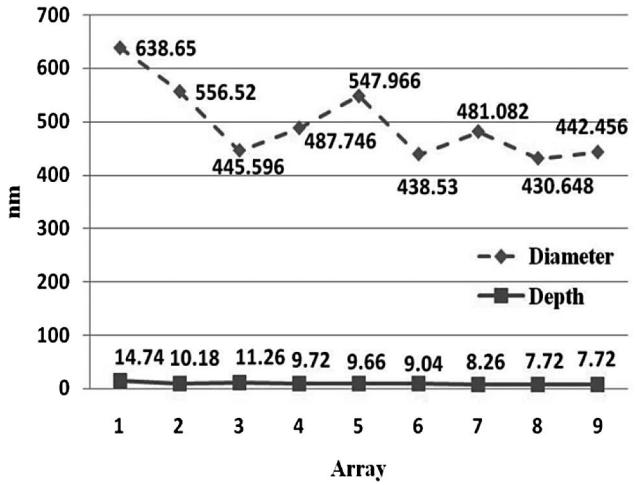

Fig. 10. Measurement result of cavity size in Chip 1 presented by mean values.

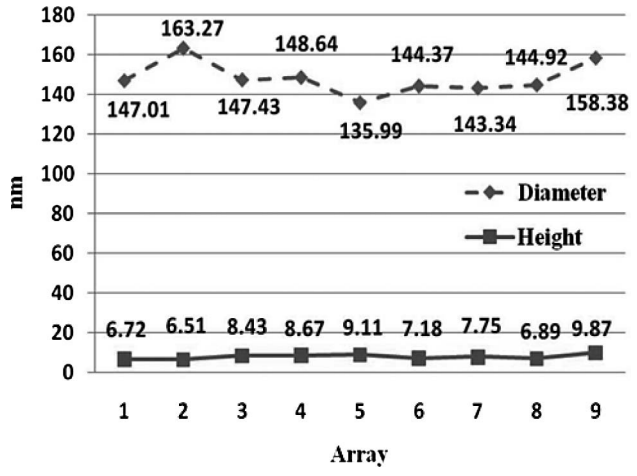

Fig. 11. Measurement result of fiber size in Chip 2 presented by mean values.

the null hypothesis is true. The fact that p values are based on this assumption is crucial to their correct interpretation. The lower the p value is, the less likely the result is, assuming the

TABLE II
CALCULATION RESULTS OF CI FOR THE SIZES OF FIBERS AND CAVITIES

CHIP 1		CONFIDENCE INTERVAL	MEAN	STD. DEV.
FIBER	DIAMETER	**[137.11 148.63]**	142.87	8.82
	HEIGHT	**[7.338 8.062]**	7.7	0.554
CAVITY	DIAMETER	**[453.03 540.12]**	496.58	66.65
	DEPTH	**[8.46 11.16]**	9.81	2.07
CHIP 2		**CONFIDENCE INTERVAL**	MEAN	STD. DEV.
FIBER	DIAMETER	**[143.13 153.17]**	148.15	7.68
	HEIGHT	**[7.18 8.62]**	7.9	1.11

All measured values are in the unit of nanometer.

TABLE III
p-VALUE CALCULATIONS AND APPLICATION

			Standard	Mean	Std.Dev.	Z	ϕ(abs(Z))	**P-Value**	Sig. Lv.	Reject
C1	A3	D	142.866	144.603	14.95	0.367	0.6736	**0.6528**	0.05	No
		H	7.707	7.61	1.79	-0.171	0.5987	**0.8026**	0.05	No
	A5	D	142.866	157.081	7.867	5.714	0.9997	**0.0006**	0.05	Yes
		H	7.707	8.37	1.442	1.454	0.9394	**0.1212**	0.05	No
C2	A3	D	148.148	147.425	8.081	1.784	0.9678	**0.0644**	0.05	No
		H	7.903	8.43	2.182	1.048	0.8531	**0.2938**	0.05	No
	A7	D	148.148	143.341	9.741	0.244	0.5987	**0.8026**	0.05	No
		H	7.903	7.75	1.067	0.203	0.5987	**0.8026**	0.05	No

C1 = Chip 1, C2 = Chip 2, D = diameter, and H = height.

null hypothesis, the more "significant" the result, in the sense of statistical significance. One often rejects a null hypothesis if the p value is less than 0.05 or 0.01, corresponding to a 5% or 1% chance, respectively, of an outcome at least that extreme, given the null hypothesis [15].

Therefore, the p value can be used to judge if a new group of measurements is reliable enough to confirm the fiber's dimension but not some other "dirty" particles on the surface. Take measurements for arrays 3 and 5 in Chip 1 and arrays 3 and 7 in Chip 2, for example, Table III gives the results of the fibers for us to tell if the measurement for each array should be accepted or rejected. In Table III, the standard is the mean of entire 90 measurements on each chip of diameter and height, respectively (see Tables I and IV); the mean is the averaged value of ten measurement for each array; the critical value Z is calculated as in (2); $\Phi(\text{abs}(Z))$ is the corresponding cumulative area, whose value can be determined by [15]; p value is obtained as in (3) and the significance level is 0.05. Thus, the rejection is able to be confirmed after comparing p value with the significance level. If p value ≤ 0.05, this group of data is rejected

$$Z = \frac{(\text{Mean} - \text{Standard}) \times \sqrt{N}}{\text{Stdev.}},\ N = 10 \qquad (2)$$

$$P\text{-Value} = 2 \times (1 - \Phi(\text{abs}(Z))). \qquad (3)$$

TABLE IV
RESULT OF MEASUREMENT FOR FIBERS ON CHIP 2

Chip 1	Array 1		Array 2		Array 3	
Meas. #	Diam.	Height	Diam.	Height	Diam.	Height
1	132.92	6.5	187.58	4.8	160.60	4.3
2	156.40	6.5	171.74	6.8	160.60	10.4
3	172.02	6.7	159.64	4.6	141.02	7
4	140.74	5.5	175.60	7	144.93	6.1
5	125.10	5.8	179.60	5.8	137.10	8.9
6	125.15	7.6	140.74	7.1	152.77	8.9
7	140.74	7.5	164.19	7.4	148.81	10.8
8	164.20	7.1	140.74	5.4	137.06	8.6
9	172.08	6.5	132.92	6	143.68	7.4
10	140.74	7.5	179.90	10.2	147.68	11.9
	Array 4		Array 5		Array 6	
	Diam.	Height	Diam.	Height	Diam.	Height
1	148.85	7.1	171.61	9.1	151.36	8.5
2	141.01	6.1	123.74	14.8	143.47	7.7
3	168.44	6.3	111.74	13.5	151.36	6.9
4	156.68	5.8	126.01	6.6	159.33	6.1
5	172.35	14.4	150.40	6.6	129.82	6.5
6	176.27	8.7	121.94	8.2	129.88	9
7	105.89	13.2	138.20	7	129.82	5.7
8	144.93	6.6	123.74	8.4	137.93	6.3
9	156.68	6.9	139.71	7	167.30	7.7
10	115.32	11.6	152.76	9.9	143.39	7.4
	Array 7		Array 8		Array 9	
	Diam.	Height	Diam.	Height	Diam.	Height
1	127.46	6.8	122.74	7.2	125.23	11.7
2	135.43	7	145.76	8.5	172.02	13
3	135.54	8.2	168.87	6.3	156.33	7.4
4	151.36	8.7	145.76	6.1	164.20	7.9
5	148.56	8.3	133.00	6.7	191.19	8.1
6	164.19	6.9	148.56	6.2	143.40	6.6
7	140.83	7.1	140.74	7.3	143.40	10.9
8	140.74	10.3	140.74	7.7	127.46	10.4
9	140.74	7	143.56	6.3	184.11	10.2
10	148.56	7.2	159.48	6.6	176.44	12.5
Overall Mean			Diameter: 148.15		Height: 7.9	

All measured values are in the unit of nanometer.

C. Discussion

The aforementioned calculations show relatively large variations to the measurement of the same objective. For example, in Table I array 2, the fourth measurement of fiber diameter is 123.72 nm, which is quite different from the sixth measurement of 160.6 nm. Similarly, the measurement of fiber height is 5.1 nm versus 10.3 nm in array 9. This phenomenon is not caused by an incorrect measurement but by the nonuniform growth of the VACNFs on Ni dot nanoelectrodes. Similarly, in Fig. 5, the upper-left differs from the bottom-right owing to an uneven distribution of the cavities generated in CMP procedure, which matters very little. The cavities in the arrays will not influence the performance of the nanofibers on the nanoelectrodes as long as the VACNFs growth is not impeded. Furthermore, as introduced in Section II-C, the bare VACNF tips we originally incubated by PECVD are supposed to have a diameter of 70 nm while our AFM measurement combined with a statistical analysis shows an almost double size after the deposition of SiO_2 and CMP steps as given in Table II. Based on this phenomenon, we may conclude that there could be some SiO_2 residual still covering these VACNF tips after CMP. Thus, there would be an obstacle to the electrical connection with outside circuit through the contact pads. This is also verified by our attempt at electrical property testing of VACNF tips using current sensing AFM. In the future, since TEOS causes the cavities on the surface of the nanoelectrodes, it could essentially be used as a method to create nanochannels for other potential applications such as chemical sensor and pH sensor Lab-on-Chip system development using the VACNFs.

V. CONCLUSION

Microchips with multiplexed 3×3 biosensing arrays employing patterned VACNFs are ready to work. However, when researchers want to examine the quality of the fabrication, a tool with nanoscale ability is needed. In this paper, the measurement of the VACNFs and the cavities with AFM are carried out and the results presented. As a result, their accurate sizes are indicated statistically by CI. Furthermore, p value is introduced as a tool for judgment of the possibility of correct measure target in the future measurement.

ACKNOWLEDGMENT

The authors would like to express their sincere gratitude to P. U. Arumugam for chip fabrication at NASA AMES and H. D. Tourtillot for her help with the experiment.

REFERENCES

[1] P. U. Arumugam, H. Chen, S. Siddiqui, J. A. P. Weinrich, A. Jejelowo, J. Li, and M. Meyyappan, "Wafer-scale fabrication of patterned carbon nanofiber nanoelectrode arrays: A route for development of multiplexed, ultrasensitive disposable biosensors," *Biosens. Bioelectron.*, vol. 24, pp. 2818–2824, 2009.

[2] National Research Council and Committee on Indicators for Waterborne Pathogens, 2004. Indicators for Waterborne Pathogens. National Academies Press, Washington, DC.

[3] K. Dill, D. D. Montgomery, A. L. Ghindilis, K. R. Schwarzkopf, S. R. Ragsdale, and A. V. Oleinikov, "Immunoassays based on electrochemical detection using microelectrode arrays: Microarrays for biodefense and environmental applications," *Biosens. Bioelectron.*, vol. 20, pp. 736–742, 2004.

[4] O. Niwa and H. Tabei, "Voltammetric measurements of reversible and quasi-reversible redox species using carbon film based interdigitated array microelectrode," *Anal. Chem.*, vol. 66, no. 2, pp. 285–289, 1994.

[5] J. Li, J. Koehne, A. M. Cassell, H. Chen, Q. Ye, H. T. Ng, J. Han, and M. Meyyappan, "Miniaturized multiplex label-free electronic chip for rapid nucleic acid analysis based on carbon nanotube nanoelectrode arrays," *J. Mater. Chem.*, vol. 14, pp. 676–684, 2004.

[6] J. Li, J. Koehne, A. M. Cassell, H. Chen, Q. Ye, H. T. Ng, J. Han, and M. Meyyappan, "Bio-nano fusion in sensor and device development," *MCB*, vol. 1, no. 1, pp. 69–80, 2004.

[7] M. A. Guillorn, T. E. McKnight, A. Melechko, V. I. Merkulov, P. F. Britt, D. W. Austin, D. H. Lowndes, and M. L. Simpson, "Individually addressable vertically aligned carbon nanofiber based electrochemical probes," *J. Appl. Phys.*, vol. 91, no. 6, pp. 3824–3828, 2002.

[8] P. He and L. Dai, "Aligned carbon nanotube-dna electrochemical sensors," *Chem. Commun.*, pp. 348–349, 2004.

[9] Y. H. Yun, V. Shanov, M. J. Schulz, Z. Dong, A. Jazieh, W. R. Heineman, H. B. Halsall, D. K. Y. Wong, A. Bange, Y. Tuf, and S. Subramaniam, "High sensitivity carbon nanotube tower electrodes," *Sens. Actuators B*, vol. 120, pp. 298–304, 2006.

[10] P. V. Gerwen, W. Laureyn, W. Laureys, G. Huyberechts, M. O. D. Beeck, K. Baert, J. Suls, W. Sansen, P. Jacobs, L. Hermans, and R. Mertens, "Nanoscaled interdigitated electrode arrays for biochemical sensors," *Sens. Actuators B*, vol. 49, pp. 73–80, 1998.

[11] F. Patolsky, G. Zheng, and C. M. Lieber, "Fabrication of Silicon nanowire devices for ultrasensitive, label-free, real-time detection of biological and chemical species," *Nat. Protoc.*, vol. 1, pp. 1711–1724, 2006.

[12] N. Yang, H. Uetsuka, E. Osawa, and C. E. Nebel, "Vertically aligned diamond nanowires for DNA sensing," *Angew. Chem. Int. Ed.*, vol. 47, pp. 5183–5185, 2008.
[13] J. Li and M. Meyyappan, *Carbon Nanotubes: Science and Applications*. Boca Raton, FL: CRC Press, 2004.
[14] A. V. Melechko, V. I. Merkulov, T. E. McKnight, M. A. Guillorn, K. L. Klein, D. H. Lowndes, and M. L. Simpson, "Large-scale synthesis of arrays of high-aspect-ratio rigid vertically aligned carbon nanofibers," *Nanotechnology*, vol. 14, pp. 1029–1035, 2003.
[15] D. Freedman, R. Pisani, and R. Purves, *Statistics*, 4th ed. New York: Norton, 2007.

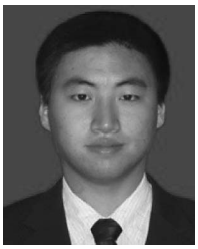

Zhuxin Dong (S'07) received the B.E. degree in biomedical engineering from Shenyang University of Technology, Shenyang, China, in 2005, the M.Phil. degree in mechanical and automation engineering from The Chinese University of Hong Kong, Hong Kong, in 2007. He is currently working toward Ph.D. degree in the Department of Mechanical Engineering, University of Arkansas, Fayetteville.

In 2005, he joined Centre for Micro and Nano Systems (CMNS), The Chinese University of Hong Kong (CUHK), where he was a member of the 3-D Digital Pen Team. His current research interests include calibration and application of microelectromechanical systems (MEMS)-based micro Intertial Measurement Unit (μIMU) for human motion sensing and recognition, application of carbon nanotube (CNT)-based nano devices, characterization and application of vertically aligned carbon nanofibers (VACNFs), and bio-MEMS.

Uchechukwu C. Wejinya (S'99–M'07) received the B.S. and M.S. degrees in electrical and computer engineering and the Ph.D. degree in electrical engineering from Michigan State University, East Lansing, in 2000, 2002 and 2007, respectively.

In 2002, he was with General Motors Research and Development Center, where he was involved in the research on magneto-rheological fluid (MRF) clutch system before returning to graduate school. After completing the Ph.D. degree, he was a Postdoctoral Researcher in the Department of Electrical and Computer Engineering, Michigan State University. Since February 2008, he has been with the Department of Mechanical Engineering, University of Arkansas, Fayetteville, where he is currently an Assistant Professor. His research interests include mechatronics with emphasis on nanotechnology, control system design and application, electronics, microtools for handling and manufacturing of micro and nanodevices, and modeling and simulation of micro and nanostructures. He is the author or coauthor of numerous conference and journal articles, and has presented at several international conferences. He was among the first group of USA graduate students to participate in the National Science Foundation, East Asia Pacific Summer Institute in Beijing, China in 2004 where he conducted research at the Chinese Academy of Sciences, Institute of Automation.

Dr. Wejinya is a member of American Society of Mechanical Engineers (ASME), National Society of Black Engineers (NSBE), and American Society for Engineering Education (ASEE). He received the Chinese Academy of Sciences Fellowship for Young International Scientist, in 2010.